

Ovarian cancer stem cells express ROR1, which can be targeted for anti-cancer-stem-cell therapy

Suping Zhang¹, Bing Cui¹, Hsien Lai, Grace Liu, Emanuela M. Ghia, George F. Widhopf II, Zhuhong Zhang, Christina C. N. Wu, Liguang Chen, Rongrong Wu, Richard Schwab, Dennis A. Carson², and Thomas J. Kipps²

Moores Cancer Center, University of California, San Diego, La Jolla, CA 92093

Contributed by Dennis A. Carson, October 22, 2014 (sent for review September 15, 2014; reviewed by Brunhilde H. Felding)

Although initially responsive to chemotherapy, many patients with ovarian cancer subsequently develop relapsed and potentially fatal metastatic disease, which is thought to develop from cancer stem cells (CSCs) that are relatively resistant to conventional therapy. Here, we show that CSCs express a type I receptor tyrosine kinase-like orphan receptor (ROR1), which is expressed during embryogenesis and by many different cancers, but not normal postpartum tissues. Ovarian cancers with high levels of ROR1 had stem cell-like gene-expression signatures. Furthermore, patients with ovarian cancers with high levels of ROR1 had higher rates of relapse and a shorter median survival than patients with ovarian cancers that expressed low-to-negligible amounts of ROR1. We found that ROR1-positive (ROR1⁺) cells isolated from primary tumor-derived xenografts (PDXs) also expressed aldehyde dehydrogenase 1 (ALDH1) and had a greater capacity to form spheroids and to engraft immune-deficient mice than did ROR1-negative (ROR1^{Neg}) ovarian cancer cells isolated from the same tumor population. Treatment with UC-961, an anti-ROR1 mAb, or shRNA silencing of ROR1 inhibited expression of the polycomb ring-finger oncogene, Bmi-1, and other genes associated with the epithelial-mesenchymal transition. Moreover, shRNA silencing of ROR1, depletion of ROR1⁺ cells, or treatment with UC-961 impaired the capacity of ovarian cancer cells to form spheroids or tumor xenografts. More importantly, treatment with anti-ROR1 affected the capacity of the xenograft to reseed a virgin mouse, indicating that targeting ROR1 may affect CSC self-renewal. Collectively, these studies indicate that ovarian CSCs express ROR1, which contributes to their capacity to form tumors, making ROR1 a potential target for the therapy of patients with ovarian cancer.

ROR1 | ovarian cancer stem cell | monoclonal antibody | PDX mice model

Although most patients with advanced ovarian cancer initially respond well to paclitaxel- and cisplatin-based therapies (1, 2), ~85% of patients relapse within a few years after systemic chemotherapy and cytoreductive surgery, including those who had an apparent complete response to therapy (3). Cancer recurrence is thought to reflect the survival of a small percentage of ovarian cancer stem cells (CSCs), which are relatively resistant to chemotherapy, can repopulate the tumor, and can spread to distal sites (4–6).

Studies have identified phenotypic and functional characteristics of CSCs that may distinguish such cells from other neoplastic cells (7, 8). Compared with other ovarian cancer cells, ovarian CSCs have relatively high aldehyde dehydrogenase (ALDH1) enzymatic activity (9–11), which may serve to detoxify intracellular aldehydes or various cytotoxic drugs (12, 13). Ovarian CSCs also can extrude small molecules, such as various chemotherapeutic drugs or fluorescent dyes, allowing for their identification as a less fluorescent “side population” in flow-cytometric analysis of tumor cells stained with the DNA-binding dye Hoechst 33342 (14–16). Furthermore, ovarian CSCs may express various surface antigens, such as CD44, CD117, or CD133 (7, 8, 17–19). Functionally, human ovarian CSCs apparently can form nonadherent cellular spheres, called “spheroids,” which in turn are enriched for ovarian cancer cells that have high ALDH1 activity, are relatively resistant to chemotherapeutic

drugs, and have enhanced potential for seeding metastatic sites or engrafting immune-deficient mice (5, 17, 18, 20–22).

Ovarian CSCs may have stem cell-like gene-expression signatures, possibly reflecting their relatively high capacity for self-renewal and capacity to regenerate the entire tumor population (4, 23). Such gene-expression signatures in turn are associated with a subset of ovarian cancers that are less well differentiated, have a higher propensity to form spheroids in vitro or metastasize in vivo, and are associated with poorer prognosis (16, 24). Finally, ovarian cancer spheroids also express genes associated with the epithelial-mesenchymal transition (EMT) that provide the traits required for invasion and metastasis (21, 25).

Another potential marker for CSCs is ROR1. ROR1 is a type I orphan-receptor tyrosine kinase-like surface protein that is found on neoplastic cells of many different types of cancer, but not on normal adult tissues (26–32). Moreover, ROR1 predominantly seems to be expressed by less well-differentiated tumors that have high potential for relapse and metastases and that also express markers associated with EMT (31, 33). Conversely, silencing ROR1 in metastasis-prone breast-cancer cell lines could attenuate expression of genes associated with EMT and impair their migration/invasion capacity in vitro and their metastatic potential in vivo (33). Very recently, Zhang et al. reported that high-level expression of ROR1 was an independent prognostic factor for predicting relatively short disease-free survival or overall survival of patients with ovarian cancer (34). In this study, we examined whether ovarian cancer cells that

Significance

This study demonstrates that the oncoembryonic surface antigen, receptor tyrosine kinase-like orphan receptor 1 (ROR1), is expressed on human ovarian cancer stem cells (CSCs), on which it seems to play a functional role in promoting migration/invasion or spheroid formation in vitro and tumor engraftment in immune-deficient mice. Treatment with a humanized mAb specific for ROR1 (UC-961) could inhibit the capacity of ovarian cancer cells to migrate, form spheroids, or engraft immune-deficient mice. Moreover, such treatment inhibited the growth of tumor xenografts, which in turn had a reduced capacity to engraft immune-deficient mice and were relatively depleted of cells with features of CSC, suggesting that treatment with UC-961 could impair CSC renewal. Collectively, these studies indicate that ovarian CSCs express ROR1, which may be targeted for anti-CSC therapy.

Author contributions: S.Z. and T.J.K. designed research; S.Z., B.C., H.L., G.L., Z.Z., C.C.N.W., L.C., and R.W. performed research; G.F.W. and R.S. contributed new reagents/analytic tools; S.Z., B.C., H.L., G.L., E.M.G., D.A.C., and T.J.K. analyzed data; and S.Z., H.L., and T.J.K. wrote the paper.

Reviewers included: B.H.F., The Scripps Research Institute.

The authors declare no conflict of interest.

Freely available online through the PNAS open access option.

¹S.Z. and B.C. contributed equally to this work.

²To whom correspondence may be addressed. Email: tkipps@ucsd.edu or dcarson@ucsd.edu.

This article contains supporting information online at www.pnas.org/lookup/suppl/doi:10.1073/pnas.1419599111/-DCSupplemental.

expressed ROR1 also had phenotypic and functional characteristics associated with ovarian CSCs.

Results

Expression of ROR1 Is Associated with Poor Prognosis and Stem Cell-Like Gene-Expression Signatures in Ovarian Cancer. We analyzed the PubMed Gene Expression Omnibus (GEO) database on ovarian cancer cells of 285 patients with epithelial ovarian, primary peritoneal, or fallopian tube cancer, which we segregated into three subgroups based upon their relative expression of *ROR1* (35). Patients with tumors having the upper-third expression level of *ROR1* mRNA (designated as ROR1^{Hi}) had a significantly shorter median progression-free survival (PFS) (1.2 y) or overall survival (OS) (3.8 y) than did patients with lower-third level (called ROR1^{Low}) (PFS = 2.2 y or OS undefined within 5 y) ($P = 0.0003$ or 0.03 , respectively) (Fig. 1A and Table S1). Although most patients included in this cohort had high-grade and advanced-stage serous cancers, there was a small subset of patients who had endometrioid ovarian cancers, serous tumors of low-grade, and/or early-stage tumors with low malignant potential (LMP) ($n = 18$) (35). We noted that these cases had a significantly lower median level of *ROR1* mRNA expression (median = 5.4) than did the other cases of this cohort (median = 6.1, $n = 267$, $P \leq 0.001$). Moreover, a significantly higher percentage of these LMP tumors (72%, $n = 13$) had expression levels of *ROR1* that placed them in the ROR1^{Low} subgroup, and a significantly lower percentage of these cases were in the ROR1^{Hi} subgroup (6%, $n = 1$) than would be expected by chance ($P < 0.0001$) (Table S2). Furthermore, segregation of high-grade, late-stage ovarian tumors, described in GSE26712 (36), another PubMed GEO database, into three subgroups by virtue of their relative expression of *ROR1* yielded similar findings, identifying patients with ROR1^{Hi} tumors as having a poorer prognosis relative to patients with ovarian cancers in the ROR1^{Low} subgroup (Fig. S1A) (36).

We ranked the 19,093 genes from the GSE9891 dataset by their relative expression level in ROR1^{Hi} versus ROR1^{Low} ovarian cancer samples for gene-set enrichment analyses (37). Compared with ROR1^{Low} samples, ROR1^{Hi} tumor samples were enriched in

expression of gene signatures associated with the “side population” (Fig. 1B, Fig. S1B, and Table S3) (16). ROR1^{Hi} tumors samples also were relatively enriched in expression of gene sets associated with human embryonic stem cells (16, 23, 24) (Fig. 1B, Fig. S1B, and Table S3). Moreover, embryonic stem cell sets of genes targeted by Nanog, Oct4, Sox2, or Nos, Nos tfs, or Myc target 1 genes were enriched or activated in the ROR1^{Hi} ovarian tumor samples relative to ROR1^{Low} samples (Fig. S1B and Table S3). In particular, we noted that four of the nine identified gene sets associated with human embryonic stem cells actually included *ROR1* (23). The genes induced by the EMT also were enriched or activated in ROR1^{Hi} tumor samples relative to ROR1^{Low} tumors (Fig. S1C). Finally, the expression level of *ALDH1A1*, encoding the CSC marker aldehyde dehydrogenase 1, was significantly higher in ROR1^{Hi} ovarian-tumor samples than in ROR1^{Low} ovarian cancer samples (Fig. S1C). However, we did not discern ROR1^{High} ovarian cancers to have relative enrichment in their expression of the 51-gene signature that could distinguish ovarian cancer samples on the basis of morphology (24). Nevertheless, these analyses revealed that high-level expression of *ROR1* may be associated with ovarian CSC.

Expression of ROR1 in Primary Ovarian Cancer Cells. We examined fresh-frozen tumor tissues from each of 14 patients with ovarian cancer for ROR1 protein via immunoblot analysis. As in our previous study using immunohistochemistry (30), we found about half of these ovarian cancers (7 out of 14, 50%) expressed high-level ROR1 by immunoblot analysis (Fig. S2A and Table S4). Similarly, we found that two of three patient-derived xenografts (PDXs) had readily detectable ROR1, as assessed via immunoblot analysis (Fig. S2B), immunohistochemistry, or flow-cytometric analysis (Fig. 2). The PDX sample AA0857 expressed higher levels of ROR1 than did AA1581, which in turn expressed higher levels of ROR1 than did OV1110, which expressed undetectable ROR1 except in a few cells (Fig. 2).

We also examined for expression of ROR1 on cells that had ALDH1 enzymatic activity, which we assessed by treating the cells with ALDEFLUOR. ALDH1 converts ALDEFLUOR into a fluorescent product that can be monitored via flow cytometry. The enhanced fluorescence of cells specifically due to the enzymatic conversion of ALDEFLUOR can be assessed by comparing the fluorescence of stained cells with that of cells stained in parallel with ALDEFLUOR and diethylaminobenzaldehyde (DEAB), an inhibitor of ALDH1-enzymatic activity. We found that the cells that were ALDEFLUOR-positive expressed higher levels of ROR1 than did the ALDEFLUOR-negative cells of the same tumor-cell populations (Fig. 2B and Fig. S2C). Conversely, ROR1⁺ cells in each of these PDX samples had higher proportions of ALDEFLUOR-staining cells than the tumor cells that did not express ROR1 (Fig. S2D).

Expression of ROR1 in Ovarian Cancer Spheroids. We cultured single-cell suspensions of primary ovarian cancer cells and monitored their capacity to form spheroids. We did not detect any spheroids in the first week of culture until after cell division had occurred (Fig. S2E). Consistent with previous reports (17, 22), the cells within such spheroids were enriched for cells that had high levels of ALDH1 expression (Fig. S2F). We found that the PDX tumor samples with high proportions of ROR1⁺ cells (e.g., AA0857) formed significantly greater numbers of spheroids than did the tumor samples with few ROR1⁺ cells (e.g., OV1110) (Fig. 3A). Moreover, the mean size of the spheroids formed by AA0857 was significantly larger than that of AA1581 or the few spheroids that developed from OV1110. We found that cells that formed spheroids were enriched for cells that expressed high levels of ROR1 relative to that of the original tumor-cell population at the initiation of culture (Fig. 3B and C).

ROR1⁺ and ROR1^{Neg} ovarian cancer cells were isolated from the AA0857 or AA1581 PDXs by staining single-cell suspensions with a noninhibitory anti-ROR1 mAb, 4A5, for FACS sorting using the gates depicted in the bottom contour plot of Fig. 3D. The sorted ROR1⁺ cancer cells formed significant greater numbers

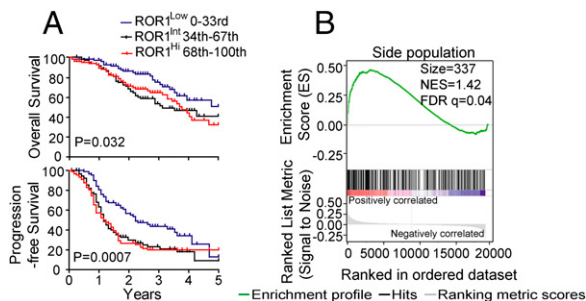


Fig. 1. Ovarian cancers that express high levels of ROR1 have stem cell-like gene-expression signatures and relatively poor prognosis. (A) Graphs were derived from published data available through the PubMed GEO database (GSE9891). Kaplan–Meier curves depict overall survival (Upper) or progression-free survival (Lower) of patients with ROR1^{Low} (blue line), ROR1^{Int} (black line), or ROR1^{Hi} (red line) ovarian cancers. The P value for the difference between ROR1^{Low} versus ROR1^{Hi} subgroups was determined by the log-rank test. (B) Enrichment plots of side-population gene-expression signatures (23) on ROR1^{Hi} tumors versus ROR1^{Low} cancers in the GSE9891 dataset. Size is the number of genes included in the analysis. NES (normalized enrichment score) accounts for the difference in gene-set size and can be used to compare the analysis results across gene sets. FDR q -val (false discovery rate q value) is the estimated probability that a gene set with a given NES represents a false positive finding. Each gene set is considered significant when the false discovery rate (FDR) is less than 25%. The middle portion of the plot shows where the members of the gene set appear in the list of ranked genes; red and blue colors represent positive and negative correlation with ROR1 expression, respectively.

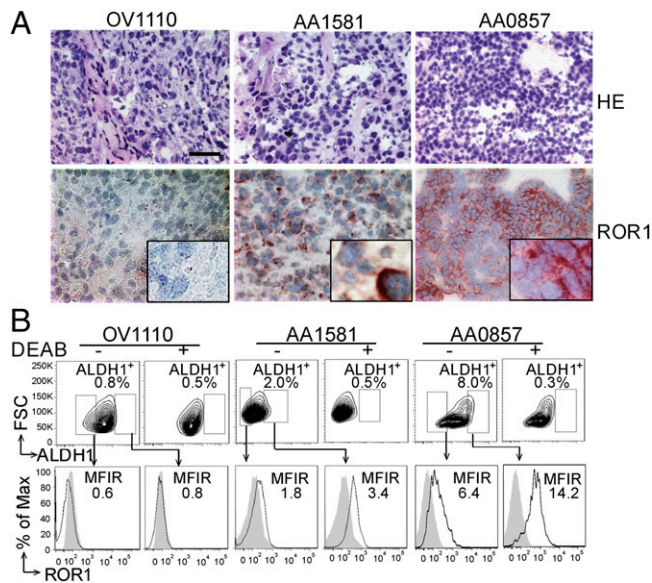


Fig. 2. ROR1 is expressed on ovarian cancer cells with high ALDH1 activity. (A) OV1110, AA1581, or AA0857 were stained with either HE (Upper) or with the anti-ROR1 mAb 4A5 (Lower). Bound 4A5 is shown in red. (Scale bar: 35 μm .) (B) Flow-cytometric analysis of OV1110, AA1581, or AA0857. The cells were stained with 4A5 or control mAb, and with ALDOFLUOR without (–) or with (+) the ALDH1 inhibitor DEAB, as indicated at the top. The open boxes in the each contour plot indicate the gates for identifying cells with ALDH1 activity, the proportion of which is indicated. The open boxes in the left of the contour plots depict the gates used to identify cells that are certain to lack ALDH1 activity. In the lower row are histograms depicting the fluorescence of cells within these boxes that were negative (left) or positive (right) for ALDH1 activity. The filled histograms depict the fluorescence of cells stained with an isotype-control mAb whereas the open histograms depict the fluorescence of cells stained with 4A5. The number in each plot provides the mean fluorescence intensity ratio (MFIR).

of spheroids and larger spheroids than ROR1^{Neg} tumor cells (Fig. 3E and Fig. S2E and G). Furthermore, sorted ROR1⁺ cancer cells were more invasive into Matrigel than the ROR1^{Neg} cancer cells isolated from the same tumor population (Fig. S3A and B).

Ovarian Cancer Cells That Express ROR1 Have Enhanced Capacity for Engraftment. PDX tumor samples with high proportions of ROR1⁺ cells (e.g., AA0857) displayed faster growth in immune-deficient mice than did the tumor samples with intermediate expression of ROR1 or few ROR1⁺ cells (e.g., OV1110) (Fig. 4A). We isolated ROR1⁺ and ROR1^{Neg} cells from AA0857 or AA1581 by FACS and performed a tumorigenicity assay in immune-deficient mice using limiting numbers of tumor cells. As shown in Table 1, as few as 500 purified ROR1⁺ cells from either AA0857 or AA1581 could initiate a tumor in most engrafted mice (Table 1). In contrast, the same number of ROR1^{Neg} tumor cells from either AA0857 or AA1581 did not form tumors except in a few animals, which developed smaller PDX tumors than did the ROR1⁺ cells (Table 1 and Fig. 4B and C). We also evaluated the capacity of ROR1⁺ versus ROR1^{Neg} cells from the AA0857 PDX population to form tumors after orthotopic transfer to the ovary. Although 500 ROR1⁺ cells could give rise to tumors in the ovary, the ROR1^{Neg} cells were not able to give rise to such tumors (Fig. 4C). Moreover, the percentage of cells in these tumors that expressed ROR1 was similar to that noted in the parental tumors (Fig. 4D), suggesting that ROR1⁺ cells were able to give rise to ROR1^{Neg} cells.

Silencing Expression of ROR1 Reduces Ovarian Cancer Cell Expression of Bmi-1 and Markers of EMT. We silenced expression of ROR1 in ovarian adenocarcinoma cell lines (e.g., SKOV3 or 2008) using

short-hairpin RNAs (shRNAs), which targeted either of two different sequences of ROR1 (31). Ovarian cancer cells transfected with ROR1-shRNAs have reduced expression of ROR1, formed significantly fewer spheroids and migrated significantly less well into Matrigel compared with the same cell lines transfected with a control shRNA (Fig. 5A and Fig. S3C and D). Furthermore, silencing ROR1 reduced expression of Bmi-1, the polycomb ring-finger oncogene that regulates CSC self-renewal (38, 39). Moreover, silencing ROR1 protein expression inhibited the expression level of EMT markers (e.g., N-cadherin and vimentin) and SNAIL1/2, master regulators of EMT (Fig. 5B). Finally, cells silenced for ROR1 lost their capacity to form tumors in immune-deficient mice (Fig. 5C).

A Humanized Antibody Specific for ROR1 Could Inhibit the Capacity of Ovarian Cancer Cells to Form Spheroids in Vitro or Engraft Immune-Deficient Mice. We developed a humanized anti-ROR1 antibody, named cirmtuzumab (UC-961), which has high binding affinity

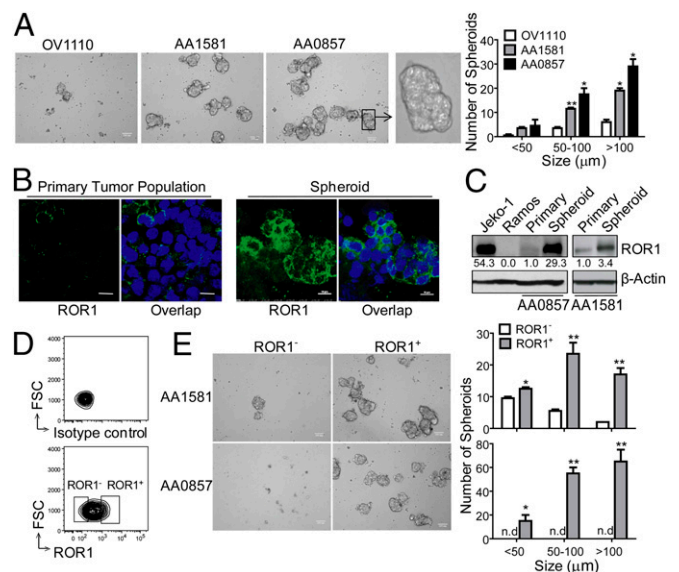
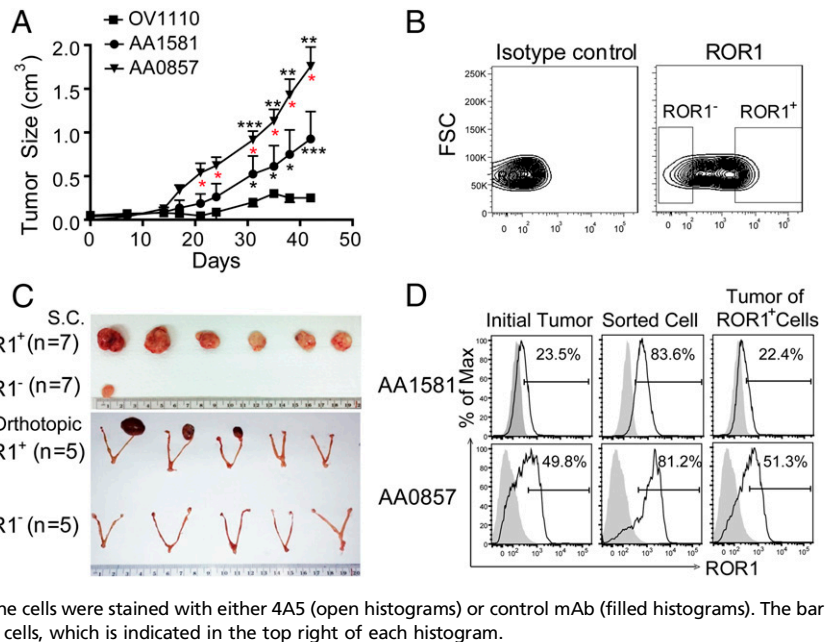


Fig. 3. ROR1⁺ cells give rise to more spheroids than ROR1^{Neg} cells. (A) Photomicrographs of spheroids that developed from cultured single cells isolated from OV1110, AA1581, or AA0857. (Scale bar: 100 μm , except for *Far Right*, which displays the spheroid in the box under higher magnification.) The bar graph to the *Right* depicts the average numbers of small (<50 μm), medium (50–100 μm), or large (>100 μm) spheroids formed by cells of OV1110 (open), AA1581 (gray), or AA0857 (black) in triplicate wells \pm SEM. Asterisks (*) indicate the statistical significance of differences in the number of spheroids of cells from OV1110 versus AA1581 or AA0857 (* P < 0.05, ** P < 0.01, using Student's *t* test). (B) Confocal microscopy of spheroids stained with 4A5 (green). Nuclear staining is in blue. (Scale bar: 10 μm .) (C) Immunoblot analyses of cell lysates prepared from cell lines Jeko-1 (ROR1⁺) or Ramos (ROR1^{Neg}), the primary tumor (Primary), or spheroids, as indicated on the top of each lane; the tumor from which the lysates were derived is indicated at the bottom. The blots were probed for ROR1 or β -Actin, as indicated on the right. The numbers between the panels provide the ratio of band intensities for blots probed with anti-ROR1 versus β -Actin, using Image J software. (D) Strategy for sorting ROR1⁺ versus ROR1^{Neg} cells. The open boxes indicate the gates used to select ROR1^{Neg} (left) or ROR1⁺ (right) cells. (E) Photomicrographs of ROR1⁺ or ROR1^{Neg} cells isolated from AA1581 (Upper) or AA0857 (Lower), as indicated on the left margin. (Scale bar: 100 μm .) The bar graph (*Right*) depicts the average numbers of small (<50 μm), medium (50–100 μm), or large (>100 μm) spheroids formed in three separate culture wells containing ROR1⁺ cells (filled bars) or ROR1^{Neg} cells (open bars), as indicated at the bottom of histograms (n.d., not detectable). Error bars indicate SEM. Asterisks (*) indicate the statistical significance of differences between the number of spheroids that formed by ROR1⁺ cells versus ROR1^{Neg} cells of AA0857 (Upper) or AA1581 (Lower) (* P < 0.05, ** P < 0.01, using Student's *t* test). FSC, forward light scatter.

Fig. 4. ROR1⁺ ovarian cancer cells more effectively engraft immune-deficient mice. (A) Tumor growth over time resulting from injection of 1×10^6 OV1110 (filled boxes), AA1581 (filled circles), or AA0857 (filled inverted triangles) per mouse. Asterisks indicate the statistical significance of differences between the mean sizes of the tumors that developed in mice engrafted with AA0857 versus OV1110 (black), AA1581 versus OV1110 (black), or AA0857 versus AA1581 (red) (* $P < 0.05$, ** $P < 0.01$, *** $P < 0.001$, using Student's *t* test, $n = 5$ for each group).

(B) Gating strategy used for sorting ROR1⁺ versus ROR1^{Neg} cells, as in Fig. 3D. (C) Photographs of representative tumors extirpated from mice engrafted with ROR1⁺ or ROR1^{Neg} ovarian cancer cells of AA0857. (Upper) Representative tumors that formed on the flanks of engrafted mice. (Lower) Ovarian tumors orthotopically implanted with sorted ROR1⁺ or ROR1^{Neg} cells. (D) The fluorescence of single-cell suspensions of unsorted tumor (Initial Tumor), freshly sorted ROR1⁺ cells before engraftment (Sorted Cell), or cells isolated from tumors that developed in mice engrafted with ROR1⁺ cells (Tumor of ROR1⁺ Cells), as indicated at the top, for cells derived from AA1581 (Upper) or AA0857 (Lower), as indicated on the left margin. The cells were stained with either 4A5 (open histograms) or control mAb (filled histograms). The bar indicates the gate used to calculate the proportion of ROR1⁺ cells, which is indicated in the top right of each histogram.



and can recognize the same epitope as D10, a lower affinity mouse mAb specific for ROR1 that had functional activity against ROR1⁺ tumor cells in vitro and in vivo (33, 40). Treatment with UC-961 blocked the capacity of AA0857 tumor cells to form spheroids and reduced their expression of ROR1 and vimentin (Fig. 6). UC-961-treated tumor cells also lost their capacity to migrate into Matrigel (Fig. S4). We examined whether treatment with UC-961 could inhibit the capacity of AA0857 cells to form tumors in immune-deficient mice. We treated mice engrafted with AA0857 cells with biweekly i.v. infusions of UC-961 (at 10 mg/kg) or control human immunoglobulin G (hIgG) and found that UC-961 significantly suppressed the development and growth of the PDX tumors (Fig. 7A–C and Fig. S5A–C).

Single-cell suspensions were made from tumors that developed in control-treated mice or the few mice among those that were treated with UC-961. Compared with the tumors that developed in control-treated mice, the tumors that developed in UC-961-treated mice had lower levels of ROR1 by immunoblot analysis (Fig. S5D), reduced proportions of ALDH1⁺ cells by flow cytometry (Fig. 7D), and reduced expression of markers associated with EMT (e.g., vimentin) (Fig. S5D). We isolated ALDH1-positive (ALDH1⁺) versus ALDH1-negative (ALDH1^{Neg}) cells from tumors that developed in mice treated with either UC-961 or control hIgG and examined their capacity to form tumors upon adoptive transfer into immune-deficient mice. As noted in prior studies (40), ALDH1⁺ cells from tumors of control-treated mice engrafted more effectively than ALDH1^{Neg} cells of the same tumor population (Fig. 7E).

Table 1. Tumor incidence in animals implanted with ROR1⁺ Or ROR1^{Neg} cells isolated from ovarian PDX samples

Tissue ID	Group	Number of cells			Frequency	P value
		5,000	1,500	500		
AA0857	ROR1 ⁺	6/6 (100%)	2/3 (67%)	6/7 (86%)	1/515	0.0004
AA0857	ROR1 ^{Neg}	4/5 (80%)	0/3 (0%)	1/7 (14%)	1/4,158	
AA1581	ROR1 ⁺	n.d.	4/5 (80%)	3/5 (60%)	1/747	0.003
AA1581	ROR1 ^{Neg}	n.d.	1/5 (20%)	0/5 (0%)	1/9,230	

Frequency of tumorigenic cell and probability estimates were computed using Extreme Limiting Dilution Analysis (ELDA) software. n.d., not done.

However, the ALDH1⁺ cells from the tumors of UC-961-treated mice did not have an apparent advantage over ALDH1^{Neg} cells in engrafting such immune-deficient mice (Fig. 7E). Moreover, the tumor cells isolated from UC-961-treated mice had lower expression of Bmi-1 and markers associated with EMT (e.g., vimentin) (Fig. S5E and F) than the tumors that developed in control-treated mice. Collectively, these data suggest that

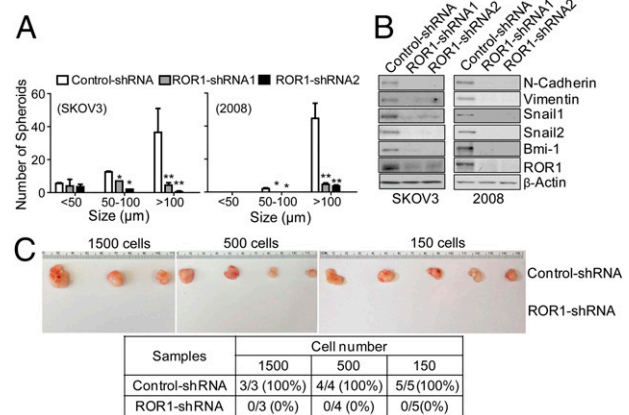


Fig. 5. Silencing ROR1 inhibits spheroid formation, tumor engraftment, and the expression of Bmi-1 or markers associated with EMT. (A) The average numbers of spheroids assessed in each of three separate wells (\pm SEM) for SKOV3 (Left) or 2008 (Right) transfected with control-shRNA (open bars), ROR1-shRNA1 (gray bars), or ROR1-shRNA2 (black bars) are depicted in the histograms, as in Fig. 3E. (B) Immunoblot analysis of lysates made from SKOV3 or 2008 transfected with control-shRNA, ROR1-shRNA1, or ROR1-shRNA2, as indicated at the top of each lane. The blots were probed for the proteins listed on the right. (C) Representative tumors extirpated from immune-deficient mice engrafted with defined numbers of 2008 cells transfected with either control-shRNA (top row) or ROR1-shRNA (bottom row). (Lower) A table providing the numbers of animals that had tumor at 5 wk post tumor-cell injection. The numbers of injected tumor cells are indicated at the top of the columns, which provide the numbers of mice that developed tumor over the number of mice injected with 2008 cells transfected with control-shRNA or ROR1-shRNA (bottom row). The percentage of injected animals that developed tumor is provided in parentheses.

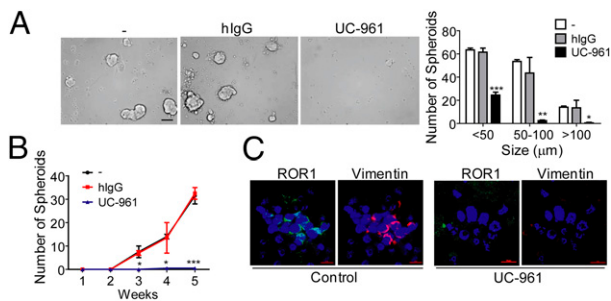


Fig. 6. ROR1 antibody UC-961 can inhibit spheroid formation of ROR1⁺ cancer cells. (A, Left) Representative images of spheroids formed by AA0857 ovarian cancer cells cultured for 3 wk in media containing control hlgG or UC-961, each at 50 μ g/mL. (Scale bar: 100 μ m.) Average numbers of spheroids formed in each of three separate wells with either treatment (\pm SEM) are indicated in the bar graph (Right), as in Fig. 3D. (B) Graph showing the average numbers of detected spheroids over time in three separate wells with either treatment (\pm SEM). (C) Confocal microscopy of ovarian cancer cell spheroids stained with mAb specific for ROR1 (green) or vimentin (red), after treatment with UC-961 for 48 h. Nuclear staining is in blue. (Scale bar: 10 μ m.)

treatment with UC-961 may inhibit the growth and self-renewal of CSC.

Discussion

Analysis of gene-expression data revealed that patients with ovarian cancers that expressed high levels of *ROR1* had a shorter median progression-free survival and overall survival than patients with tumors that had low-level expression of *ROR1*. Moreover, cases of ovarian cancer that had low malignant potential generally had low-to-negligible expression of *ROR1*. Consistent with these observations, we noted that ovarian cancers that expressed ROR1 by immunohistochemistry more commonly had a high-grade, less-differentiated histology (30), which typically is associated with aggressive disease (41). This also is consistent with a recently published study indicating that high-level expression of ROR1, assessed by immunohistochemistry of primary tumor tissue, was an independent prognostic factor for predicting relatively short disease-free survival or overall survival of patients with ovarian cancer (34).

We found ovarian cancers that expressed high levels of *ROR1* had gene-expression signatures associated with CSCs. Compared with ROR1^{Low} cases, ROR1^{Hi} ovarian cancers had higher expression of gene signatures associated with the side population, which may contain CSCs (42). Moreover, ROR1^{Hi} ovarian cancers were enriched for expression of genes associated with embryonic stem cells and EMT (17, 25), which facilitates the capacity of tumor cells to migrate and seed metastatic sites (21, 43). We also observed that two primary ovarian cancers that expressed *ROR1* were better able to grow as xenografts in immune-deficient mice than one that lacked expression of *ROR1*. Furthermore, within any one tumor population, the cells that expressed ALDH1, a marker of ovarian CSCs, expressed higher levels of ROR1, as did ovarian cancer cells that formed tumor spheroids, a functional characteristic associated with CSCs and EMT (43). Finally, we found that ROR1⁺ cells were better able to form spheroids, invade ECM, or engraft immune-deficient mice than ROR1^{Neg} cells from the same tumor population. Collectively, these studies indicate that ovarian CSCs may express relatively high levels of ROR1.

Prior studies found that expression of ROR1 could enhance tumor-cell proliferation, migration/invasion, and tumorigenicity (30, 33, 40). Conversely, silencing *ROR1*, or treatment with an anti-ROR1 mAb, could enhance apoptosis, inhibit cell proliferation and migration/invasion, and reduce the capacity of tumor cells to develop metastatic foci (30, 31, 33). Similarly, silencing ROR1 could inhibit the capacity of primary ovarian cancer cells to form spheroids, invade ECM, or to develop tumor xenografts, which are functional characteristics associated with

CSCs. As such, the present study demonstrates that ovarian CSCs also may have a dependency upon ROR1.

In the present study, we examined whether UC-961 could target ovarian CSCs. UC-961 is a humanized IgG1 mAb currently in clinical trials that binds with high affinity to the same epitope of ROR1 as the low-affinity mAb D10, which, in prior studies, was found capable of down-modulating ROR1, impairing ROR1⁺ leukemia-cell engraftment, and inhibiting breast-cancer cell metastasis (33, 40). We found that treatment of primary ovarian PDX tumor cells with an anti-ROR1 mAb, UC-961, could inhibit spheroid formation and migration in vitro and engraftment in immune-deficient mice. Furthermore, the small tumors that did develop in mice treated with UC-961 had reduced expression of Bmi-1, ALDH1, ROR1, and genes associated with EMT. Moreover, treatment with anti-ROR1 impaired the capacity of tumor xenografts to re-engage a virgin mouse. These studies suggest that treatment with this anti-ROR1 mAb could impair the self-renewal capacity of CSC cells in vivo. As such, these studies demonstrate that UC-961 might inhibit the maintenance and/or self-renewal of ovarian CSCs, which otherwise may be resistant to chemotherapy and responsible for relapse after conventional anticancer treatment (4–6).

Although several putative ovarian CSC markers have been identified (e.g., CD133, ALDH1, CD44, and CD117) (8, 18, 19, 44, 45), such markers also can be found on normal adult tissues, including normal stem cells (10, 46, 47). Therefore, targeting such antigens with mAbs or small molecules also may affect the normal tissues that express these antigens (48, 49). However, with few exceptions (50), the postpartum expression of ROR1 seems restricted to cancer cells. Furthermore, due to its apparent functional role in promoting tumor-cell growth, metastasis, and tumor initiation, ROR1 seems to be a promising target for specific therapy directed against ovarian CSCs.

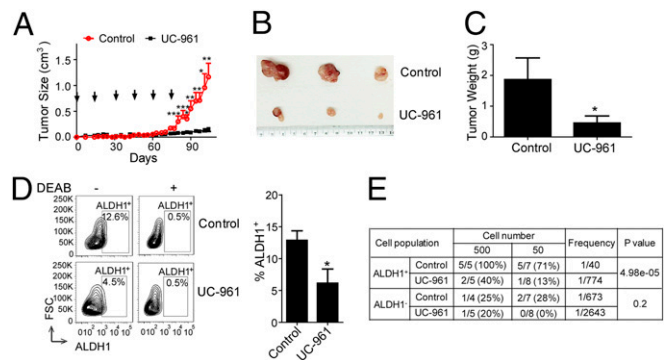


Fig. 7. ROR1 MAb inhibits tumor engraftment. (A) AA0857 cells (2.5×10^4) were engrafted into Rag2^{-/-} γ c^{-/-} mice, which were subsequently treated with control hlgG or UC-961 at times indicated by the arrows. The line graph provides the mean tumor volume over time of control hlgG-treated (red) or UC-961-treated (black) mice \pm SEM ($n = 3$ for each group). Asterisks indicate a significant difference between the mean volume measured in control-treated versus UC-961-treated mice (* $P < 0.05$, ** $P < 0.01$, *** $P < 0.001$, using Student's *t* test). (B) Representative images of tumors extirpated from mice treated with control hlgG (Upper) or UC-961 (Lower). (C) Average weights of extirpated tumors from mice treated with control hlgG or UC-961 ($n = 3$). Error bars indicate SEM. (D) Flow-cytometric analysis of cells isolated from tumors extirpated from mice treated with either control hlgG or UC-961 upon staining with ALDOFLUOR \pm the ALDH1-inhibitor DEAB, as indicated at the top of each contour plot. The box in the contour plot indicates the gate used to detect cells with ALDH1 activity. The bar graph (Right) provides the average proportion of ALDOFLUOR-staining cells in each tumor population ($n = 3$) with error bars indicating the SEM. (E) Single-cell suspensions of tumors from AA0857-engrafted immune-deficient mice that were treated with either a control antibody or UC-961 were sorted into ALDH1⁺ versus ALDH1^{Neg} subgroups by FACS. Defined numbers of ALDH1⁺ or ALDH1^{Neg} human tumor cells were engrafted into immune-deficient mice, and the development of tumor xenografts was assessed up to 5 mo postengraftment. Frequency of tumorigenic cell and probability estimates were computed using ELDA software.

Materials and Methods

Primary ovarian-tumor specimens were collected from patients, who provided written informed consent on a protocol approved by the Institutional Review Board of the University of California, San Diego (HRPP 090401), in accordance with the Declaration of Helsinki. The animal study protocol was approved by the University of California, San Diego and Medical Experimental Animal Care Committee. The PDX models were established using mechanically minced fresh ovarian cancer specimens. Early passages (1–5) of primary-tumor tissues from these PDX models were mechanically minced and enzymatically and mechanically dissociated using GentleMACS Dissociator (Miltenyi Biotec) in accordance to the manufacturer's protocol. Dead cells and erythrocytes were removed

through density gradient centrifugation using Percoll Plus (CC-17-5442-01; GE Healthcare Life Sciences) following the manufacturer's protocol.

ACKNOWLEDGMENTS. We thank Dennis Young for flow-cytometry analysis and sorting, the University of California, San Diego (UCSD) Histology Core laboratory for technical help with processing tissue specimens, Dr. Nissi Varki for histology and immunohistochemistry assessments, UCSD Moores Cancer Center Biorepository and Tissue Technology Shared Resource for PDX samples, and Dr. Lei Bao for statistical analysis assistance. This study was supported by NIH Grant P01-CA081534, the California Institute for Regenerative Medicine, and the Blood Cancer Research Fund, UCSD Foundation, Cancer Center Support Grant P30CA23100.

- McGuire WP, et al. (1996) Cyclophosphamide and cisplatin compared with paclitaxel and cisplatin in patients with stage III and stage IV ovarian cancer. *N Engl J Med* 334(1):1–6.
- Bookman MA, et al. (1996) Carboplatin and paclitaxel in ovarian carcinoma: A phase I study of the Gynecologic Oncology Group. *J Clin Oncol* 14(6):1895–1902.
- Pliarhoupoulou K, Pectasides D (2011) Epithelial ovarian cancer: Focus on targeted therapy. *Crit Rev Oncol Hematol* 79(1):17–23.
- Clarke MF, et al. (2006) Cancer stem cells—perspectives on current status and future directions: AACR Workshop on cancer stem cells. *Cancer Res* 66(19):9339–9344.
- Alvero AB, et al. (2009) Molecular phenotyping of human ovarian cancer stem cells unravels the mechanisms for repair and chemoresistance. *Cell Cycle* 8(1):158–166.
- Curley MD, Garrett LA, Schorge JO, Foster R, Rueda BR (2011) Evidence for cancer stem cells contributing to the pathogenesis of ovarian cancer. *Front Biosci (Landmark Ed)* 16:368–392.
- Baba T, et al. (2009) Epigenetic regulation of CD133 and tumorigenicity of CD133+ ovarian cancer cells. *Oncogene* 28(2):209–218.
- Curley MD, et al. (2009) CD133 expression defines a tumor initiating cell population in primary human ovarian cancer. *Stem Cells* 27(12):2875–2883.
- Landen CN, Jr, et al. (2010) Targeting aldehyde dehydrogenase cancer stem cells in ovarian cancer. *Mol Cancer Ther* 9(12):3186–3199.
- Deng S, et al. (2010) Distinct expression levels and patterns of stem cell marker, aldehyde dehydrogenase isof orm 1 (ALDH1), in human epithelial cancers. *PLoS ONE* 5(4):e10277.
- Penumatsa K, Edassery SL, Barua A, Bradaric MJ, Luborsky JL (2010) Differential expression of aldehyde dehydrogenase 1a1 (ALDH1) in normal ovary and serous ovarian tumors. *J Ovarian Res* 3:28.
- Yoshida A, Rzhetsky A, Hsu LC, Chang C (1998) Human aldehyde dehydrogenase gene family. *Eur J Biochem* 251(3):549–557.
- Alison MR, Lim SM, Nicholson LJ (2011) Cancer stem cells: Problems for therapy? *J Pathol* 223(2):147–161.
- Szotek PP, et al. (2006) Ovarian cancer side population defines cells with stem cell-like characteristics and Mullerian Inhibiting Substance responsiveness. *Proc Natl Acad Sci USA* 103(30):11154–11159.
- Moserle L, et al. (2008) The side population of ovarian cancer cells is a primary target of IFN- α antitumor effects. *Cancer Res* 68(14):5658–5668.
- Vathipadiekal V, et al. (2012) Identification of a potential ovarian cancer stem cell gene expression profile from advanced stage papillary serous ovarian cancer. *PLoS ONE* 7(1):e29079.
- Wang YC, et al. (2012) ALDH1-bright epithelial ovarian cancer cells are associated with CD44 expression, drug resistance, and poor clinical outcome. *Am J Pathol* 180(3):1159–1169.
- Zhang S, et al. (2008) Identification and characterization of ovarian cancer-initiating cells from primary human tumors. *Cancer Res* 68(11):4311–4320.
- Ferrandina G, et al. (2009) CD133 antigen expression in ovarian cancer. *BMC Cancer* 9:221.
- Abubaker K, et al. (2013) Short-term single treatment of chemotherapy results in the enrichment of ovarian cancer stem cell-like cells leading to an increased tumor burden. *Mol Cancer* 12:24.
- Davidowitz RA, et al. (2014) Mesenchymal gene program-expressing ovarian cancer spheroids exhibit enhanced mesothelial clearance. *J Clin Invest* 124(6):2611–2625.
- Liao J, et al. (2014) Ovarian cancer spheroid cells with stem cell-like properties contribute to tumor generation, metastasis and chemotherapy resistance through hypoxia-resistant metabolism. *PLoS ONE* 9(1):e84941.
- Ben-Porath I, et al. (2008) An embryonic stem cell-like gene expression signature in poorly differentiated aggressive human tumors. *Nat Genet* 40(5):499–507.
- Schwede M, et al. (2013) Stem cell-like gene expression in ovarian cancer predicts type II subtype and prognosis. *PLoS ONE* 8(3):e57799.
- Scheel C, Weinberg RA (2012) Cancer stem cells and epithelial-mesenchymal transition: Concepts and molecular links. *Semin Cancer Biol* 22(5-6):396–403.
- Fukuda T, et al. (2008) Antisera induced by infusions of autologous Ad-CD154-leukemia B cells identify ROR1 as an oncofetal antigen and receptor for Wnt5a. *Proc Natl Acad Sci USA* 105(8):3047–3052.
- Rabbani H, et al. (2010) Expression of ROR1 in patients with renal cancer: A potential diagnostic marker. *Iran Biomed J* 14(3):77–82.
- Barna G, et al. (2011) ROR1 expression is not a unique marker of CLL. *Hematol Oncol* 29(1):17–21.
- Gentile A, Lazzari L, Benvenuti S, Trusolino L, Comoglio PM (2011) Ror1 is a pseudokinase that is crucial for Met-driven tumorigenesis. *Cancer Res* 71(8):3132–3141.
- Zhang S, et al. (2012) The onco-embryonic antigen ROR1 is expressed by a variety of human cancers. *Am J Pathol* 181(6):1903–1910.
- Zhang S, et al. (2012) ROR1 is expressed in human breast cancer and associated with enhanced tumor-cell growth. *PLoS ONE* 7(3):e31127.
- Yamaguchi T, et al. (2012) NKX2-1/TTF1/TF-1-Induced ROR1 is required to sustain EGFR survival signaling in lung adenocarcinoma. *Cancer Cell* 21(3):348–361.
- Cui B, et al. (2013) Targeting ROR1 inhibits epithelial-mesenchymal transition and metastasis. *Cancer Res* 73(12):3649–3660.
- Zhang H, et al. (2014) ROR1 expression correlated with poor clinical outcome in human ovarian cancer. *Sci Rep* 4:5811.
- Tothill RW, et al.; Australian Ovarian Cancer Study Group (2008) Novel molecular subtypes of serous and endometrioid ovarian cancer linked to clinical outcome. *Clin Cancer Res* 14(16):5198–5208.
- Bonome T, et al. (2008) A gene signature predicting for survival in suboptimally debulked patients with ovarian cancer. *Cancer Res* 68(13):5478–5486.
- Subramanian A, et al. (2005) Gene set enrichment analysis: A knowledge-based approach for interpreting genome-wide expression profiles. *Proc Natl Acad Sci USA* 102(43):15545–15550.
- Park IK, Morrison SJ, Clarke MF (2004) Bmi1, stem cells, and senescence regulation. *J Clin Invest* 113(2):175–179.
- Kreso A, et al. (2014) Self-renewal as a therapeutic target in human colorectal cancer. *Nat Med* 20(1):29–36.
- Widhopf GF, 2nd, et al. (2014) ROR1 can interact with TCL1 and enhance leukemogenesis in E μ -TCL1 transgenic mice. *Proc Natl Acad Sci USA* 111(2):793–798.
- Winter WE, 3rd, et al.; Gynecologic Oncology Group Study (2007) Prognostic factors for stage III epithelial ovarian cancer: A Gynecologic Oncology Group Study. *J Clin Oncol* 25(24):3621–3627.
- Rizzo S, et al. (2011) Ovarian cancer stem cell-like side populations are enriched following chemotherapy and overexpress EZH2. *Mol Cancer Ther* 10(2):325–335.
- Vinogradov S, Wei X (2012) Cancer stem cells and drug resistance: The potential of nanomedicine. *Nanomedicine (Lond)* 7(4):597–615.
- Ricci F, et al. (2013) ALDH enzymatic activity and CD133 positivity and response to chemotherapy in ovarian cancer patients. *Am J Cancer Res* 3(2):221–229.
- Silva IA, et al. (2011) Aldehyde dehydrogenase in combination with CD133 defines angiogenic ovarian cancer stem cells that portend poor patient survival. *Cancer Res* 71(11):3991–4001.
- Bauer N, et al. (2008) New insights into the cell biology of hematopoietic progenitors by studying prominin-1 (CD133). *Cells Tissues Organs* 188(1-2):127–138.
- Arber DA, Tamayo R, Weiss LM (1998) Paraffin section detection of the c-kit gene product (CD117) in human tissues: Value in the diagnosis of mast cell disorders. *Hum Pathol* 29(5):498–504.
- Slomiany MG, et al. (2009) Inhibition of functional hyaluronan-CD44 interactions in CD133-positive primary human ovarian carcinoma cells by small hyaluronan oligosaccharides. *Clin Cancer Res* 15(24):7593–7601.
- Casagrande F, et al. (2011) Eradication of chemotherapy-resistant CD44+ human ovarian cancer stem cells in mice by intraperitoneal administration of Clostridium perfringens enterotoxin. *Cancer* 117(24):5519–5528.
- Broom HE, Rassenti LZ, Wang HY, Meyer LM, Kipps TJ (2011) ROR1 is expressed on hematogones (non-neoplastic human B-lymphocyte precursors) and a minority of precursor-B acute lymphoblastic leukemia. *Leuk Res* 35(10):1390–1394.

Supporting Information

Zhang et al. 10.1073/pnas.1419599111

SI Materials and Methods

Ovarian Cancer Cell Lines. Ovarian cancer cell lines, 2008 and SKOV3, were purchased from the American Type Culture Collection (ATCC) and cultured at 37 °C in a 5% CO₂/95% humidified air incubator in Dulbecco's modified Eagle medium (DMEM) (Invitrogen) with 10% (vol/vol) FBS (Invitrogen), 50 µg of penicillin G, and 50 µg of streptomycin sulfate. We added puromycin (1 µg/mL) to the cells transduced with lentivirus encoding control shRNA or ROR1-shRNAs, as described in the previous study (1). Stable transfectants were selected by flow cytometry.

Gene-Set Enrichment Analysis. Publicly available gene expression data of 285 ovarian cancer samples were downloaded from the Gene Expression Omnibus (GEO) database (accession number GSE9891). Of these cases, upper-third (95, ROR1^{Hi}) had highest levels of ROR1 expression whereas lower-third (95, ROR1^{Low}) had lowest levels of ROR1 expression. Using a gene-set enrichment analysis (GSEA) signal-to-noise ratio ranking metric, we ranked 19,093 genes by their association with the ovarian cancer groups (ROR1^{Hi} vs. ROR1^{Low}). We tested 11 different previously published gene sets (2–4) for their association to the ROR1 high ovarian cancer group. Such gene sets were selected for their association to either stem-like gene signatures in ovarian cancer or human embryonic stem cell identity. Each gene set was considered significant when the false discovery rate (FDR) was less than 25%. For each gene set tested, the gene-set size, the enrichment score (ES), the normalized ES (NES), the nominal *P* value (NOM *P*-val), and the FDR *q* value (FDR *q*-val) are shown. The FDR *q* value is adjusted for gene-set size and multiple hypotheses testing.

Animal Models. Four- to 8-wk-old female Rag2^{-/-}γc^{-/-} or NOD/SCID mice were used in this study, following the care and use of laboratory animal guidelines of the National Institutes of Health (NIH). The mice were housed in laminar-flow cabinets under specific pathogen-free conditions and fed ad libitum.

For the tumorigenicity assay on the flank of mice, various numbers of FACS-purified cells or cultured cell lines were suspended in mammary epithelial basal medium (MEBM) growth medium, mixed with Matrigel (BD Biosciences) at a 1:1 ratio and then transplanted s.c. into NOD/SCID mice. Tumor formation was monitored weekly. The orthotopic model was established following previously described protocol by Shaw et al. (5). In brief, viable tumor cells were suspended in MEBM growth medium. Under isoflurane-induced anesthesia, Rag2^{-/-}γc^{-/-} mice were subjected to a lateral laparotomy, the ovaries were exposed, and 5 µL of cells were injected into the ovaries using a 30G needle. Tumor growth was monitored 2–3 times per week.

To test the effect of UC-961 on primary ovarian-tumor cell engraftment, AA0857 primary cells were injected s.c. into the flank of 4- to 6-wk-old Rag2^{-/-}γc^{-/-} mice. Then, 10 mg/kg UC-961 were injected i.v. biweekly. Control groups were injected with hIgG. The tumor volume was determined using the formula $v = (\text{length}) \times (\text{width}^2) \times (0.4)$.

Spheroid-Formation Assay. The 300–10,000 single viable cells were plated on Ultra Low Attachment six-well plates (Corning Incorporated Life Sciences) and cultured in MEBM growth medium supplemented with various growth factors for 2–3 wk.

The number of spheroids was counted under an inverted microscope (Nikon).

Flow-Cytometry Analysis. Single-cell suspensions were generated from primary tumors. The numbers of viable cells were counted, treated with Fc-blocking reagent (Miltenyi Biotec; BD Pharmingen), and then stained with Alexa-647-conjugated 4A5 (6), phycoerythrin (PE)-conjugated anti-epithelial cell adhesion molecule (EpCAM), and biotin-labeled anti-H-2K^d (BD Biosciences). Phycoerythrin-Cy7-conjugated streptavidin (PE-Cy7; BD Pharmingen) was then used to detect bound anti-H-2K^d. To detect cells with ALDH1 activity, single-cell suspensions made from primary tumors were incubated with ALDEFLUOR {boron, [N-(2,2-diethoxyethyl)-5-[(3,5-dimethyl-2H-pyrrol-2-ylidene-KN)methyl]-1H-pyrrole-2-propanamido KN1] difluoro-, (T-4)-(9CI); StemCell Technologies}. Half of the cells concomitantly were treated with diethylaminobenzaldehyde (DEAB) at 50 mmol/L to inhibit ALDH1 activity and to define the gating strategy to define cells with ALDH1 activity. The “test” and “control” samples were incubated for 30–60 min at 37 °C and then analyzed with a flow cytometer (FACS-Calibur or FACS-Aria; Becton Dickinson). Data were analyzed using the FlowJo software (Tree Star). Gating was established first using forward light scatter (FSC) and side light scatter (SSC) gating to exclude cell debris. Furthermore, we excluded cells staining with propidium iodide (PI) (Sigma) but included cells staining with fluorescein diacetate (FDA) (Life Technology) to gate on viable cells. We also excluded cells staining with mAb specific for H-2K^d to exclude mouse cells. Finally, mAb specific for EpCAM allowed us to gate ovarian epithelial cells.

Cell-Invasion Assay. The 5×10^4 viable single cells from primary tumors were suspended in MEBM growth medium, plated in invasion chambers (8-µm pore size; BD Biosciences), and cultured overnight. The lower chambers were filled with serum-free, conditioned medium collected from NIH 3T3 cells. The cells on the apical side of each insert were scraped off. Invasive cells were fixed with 4% (wt/vol) paraformaldehyde and stained by Diff-Quick staining kits (IMEB Inc.) and visualized with a Nikon inverted microscope.

Immunofluorescence and Immunohistochemistry Staining. Primary tumors excised from mouse xenografts were snap-frozen in Optimal Cutting Temperature (OCT) compound for subsequent histological examination. Tissue sections were prepared and stained with hematoxylin/eosin (H&E) or 8 µg/mL 4A5 mAb using previously described protocol (1). Images were collected using a Delta Vision microscope.

For immunofluorescence analysis, Cytospin slides were prepared and first stained with the 4A5 mAb and then fixed with 4% paraformaldehyde, permeabilized in 0.1% Triton X-100, and blocked with 3% (wt/vol) BSA. Intracellular markers were stained with anti-ALDH1 (Abcam) or anti-Vimentin (Cell Signaling Technology) followed by anti-mouse IgG conjugated with Alexa Fluor 488 and/or anti-rabbit IgG conjugated with Alexa Fluor 594 (Invitrogen). The cell nuclei were stained with 4',6-diamidino-2-phenylindole (DAPI). Fluorescence images were obtained using a laser-scanning confocal imaging system (Nikon A1R Confocal Storm superresolution system).

Immunoblot Analyses. Cells isolated from primary tumor tissues, cell lines, or spheroids were lysed in buffer containing 1% Nonidet P-40, 0.1% SDS, and 0.5% sodium deoxyolate supplemented with protease inhibitors (Pierce). Size-separated proteins were transferred to

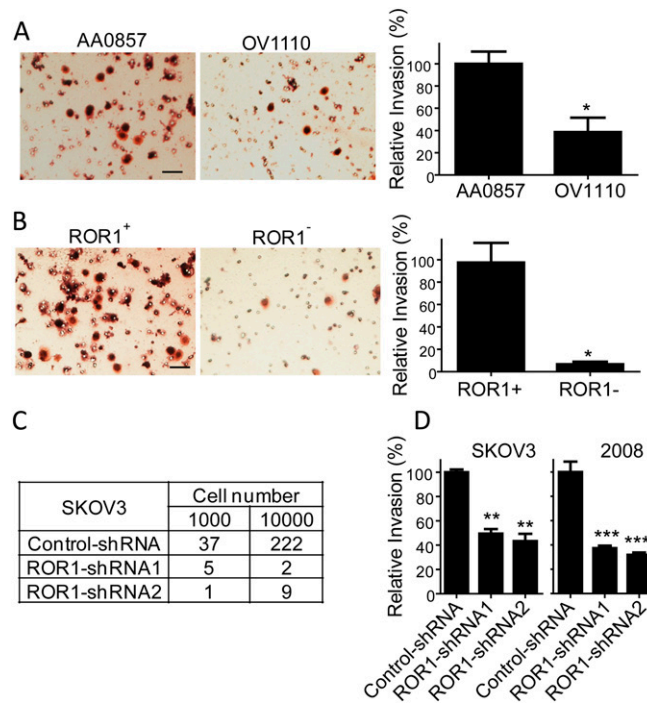


Fig. 53. ROR1⁺ ovarian cancer cells are more invasive than ROR1^{Neg} cancer cells. (A and B) Representative photomicrographs of single-cell suspensions of ROR1^{Hi} AA0857 or ROR1^{Low} OV1110 cells (A) or sorted ROR1⁺ versus ROR1^{Neg} cells isolated from AA0857 (B) after the cells were allowed to migrate into Matrigel. (Scale bar: 100 μ m.) To the *Right* of the photomicrographs are bar graphs depicting the mean relative invasion of cells into Matrigel \pm SEM of each of the cell preparations in three independent experiments, normalized to AA0857 cells (A) or sorted ROR1⁺ cells (B). (C) The average numbers of large (>100 μ m) spheroids formed by defined numbers of SKOV3 cells transduced with either control shRNA or ROR1-shRNAs in triplicate wells are shown. (D) Relative invasive capacity of SKOV3 cells expressing control shRNA or ROR1-shRNAs (*Left*) or 2008 cells expressing control shRNA or ROR1-shRNAs (*Right*) normalized to the number of Matrigel-invading cells of the control shRNA-transduced cells. Data are shown as mean of results from three independent experiment \pm SEM ($n = 3$). Asterisks are used to indicate the significance of the differences between the test-cell preparation and the cell preparation used to normalize the relative invasiveness into Matrigel (* $P < 0.05$, ** $P < 0.01$, *** $P < 0.001$ as determined via either Student's t test (A and B) or Dunnett's multiple comparison test (C and D).

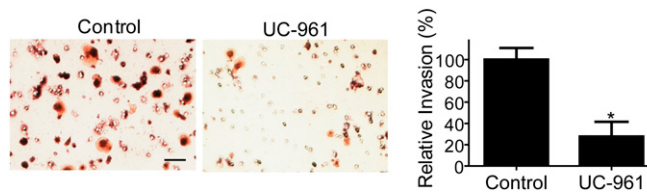


Fig. 54. UC-961 inhibits tumor-cell invasion. Representative photomicrographs of invasion of primary cells (AA0857) after treatment with control or UC-961 overnight. (Scale bar: 100 μ m.) The bar graph (*Right*) provides the average relative invasiveness normalized to that of the cells treated with the control hIgG in three independent experiments \pm SEM ($n = 3$). An asterisk * indicates $P < 0.05$ as determined by the Student t test.

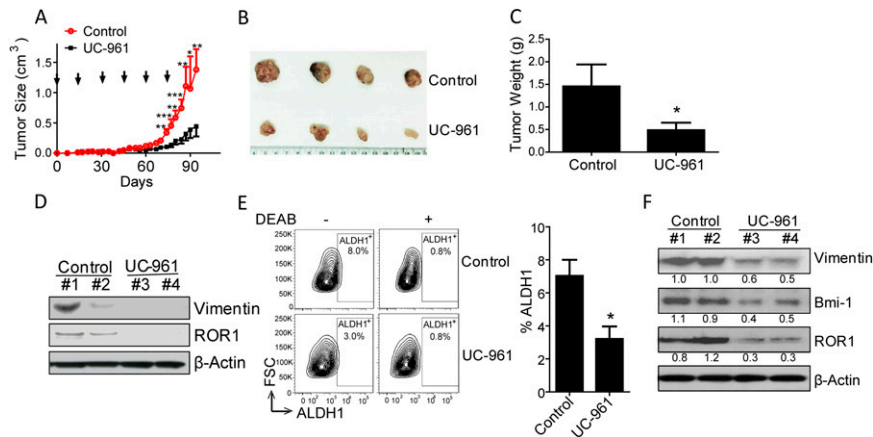


Fig. S5. ROR1 mAb inhibits tumor engraftment. (A) AA0857 cells (1×10^5) were engrafted into Rag2^{-/-}γc^{-/-} mice, which subsequently were treated biweekly with control hlgG or UC-961 (at 10 mg/kg). Tumor volume was monitored over time. The line graph provides the mean tumor volume over time of control hlgG-treated (red) or UC-961-treated (black) mice \pm SEM. Asterisks indicate a significant difference between the mean volume measured in control-treated versus UC-961-treated mice (* <0.05 , ** <0.01 , *** <0.001 by Student's *t* test). (B) Representative images of tumors extirpated from mice treated with control hlgG (Upper) or UC-961 (Lower). (C) Average weight of extirpated tumors from mice treated with control hlgG or UC-961. Error bars indicate SEM. (D) Immunoblot analyses of lysates made from tumor cells isolated from different mice treated with control hlgG (control, samples #1 and #2; UC-961, samples #3 and #4) and probed with mAb specific for Vimentin (Top), ROR1 (Middle), or β -Actin (Bottom). (E) Single-cell suspensions, obtained from tumor cells (AA0857) that were transplanted in mice receiving either control antibody or UC-961 treatment, were segregated into ALDH1⁺ versus ALDH1⁻ groups by FACS. Different numbers of cells were injected into mice. Single cells isolated from tumors in mice of second transplantation were stained for ALDEFLUOR with or without DEAB. (Left) Representative contour plot for ALDH1 activity with or without DEAB. Percentage of ALDH1⁺ population were identified based on DEAB treatment. Bar graph in the Right panel provides mean ALDH1⁺ population of tumor cells from different mice ($n = 3-5$) \pm SEM (* $P < 0.05$ as determined by Student's *t* test). (F) Cells from control or UC-961 treated group from second transplantation experiment were lysed and then subjected to immunoblot analysis for various proteins as indicated on the right margin. Data were quantified with Image J and normalized to β -Actin.

Table S1. High-level expression of ROR1 is associated with relatively poor prognosis in patients with ovarian cancer

Dataset	Group	Median survival, y	Hazard ratio	<i>P</i> value	
GSE9891	PFS	ROR1 ^{Hi}	1.2	2.0 (1.4, 3.0)	0.0003
		ROR1 ^{Low}	2.2		
	PFS (no LMP)	ROR1 ^{Hi}	1.2	1.8 (1.2, 2.7)	0.002
		ROR1 ^{Low}	2.1		
	OS	ROR1 ^{Hi}	3.7	1.7 (1.0, 2.8)	<0.05
		ROR1 ^{Low}	ND		
GSE26712	OS (No LMP)	ROR1 ^{Hi}	3.7	1.5 (0.9, 2.5)	0.09
		ROR1 ^{Low}	4.8		
	OS	ROR1 ^{Hi}	2.8	1.7 (1.1, 2.8)	<0.05
	ROR1 ^{Low}	4.7			

OS, overall survival; PFS, progression-free survival; no LMP, the dataset did not include LMP samples. Statistical differences were determined by log-rank test. ND, not defined.

Table S2. Distribution of ovarian cancers with low malignant potential (LMP) or the remaining cases of high-grade and/or advanced ovarian cancers (MAL)

Group	LMP, % (N)	MAL, % (N)	<i>P</i> value
ROR1 ^{Low}	72 (13)	31 (82)	<0.0001
ROR1 ^{Int}	22 (4)	34 (91)	
ROR1 ^{Hi}	6 (1)	35 (93)	

The entire cohort is segregated into three subgroups based upon their relative expression of ROR1. LMP denotes low malignant potential (LMP). MAL tumors were high-grade and advanced-stage serous cancers of the ovary, fallopian tube, and peritoneum. *N*, number of cases. *P* value was determined by χ^2 .

Table S3. Gene-set enrichment analysis (GSEA) of 11 stem-cell gene-expression signatures

Gene sets	Size	ES	NES	NOM <i>P</i> -val	FDR q-val	Refs.
Side population	337	0.45	1.42	0.04	0.04	2
Stem cell	46	-0.31	-0.83	0.82	0.74	4
Es exp1	335	0.25	0.78	0.84	0.85	3
Es exp2	28	-0.36	-0.85	0.66	1.00	3
Nanog targets*	854	0.35	1.44	0.01	0.04	3
Oct4 targets*	261	0.42	1.46	0.01	0.04	3
Sox2 targets*	644	0.33	1.30	0.06	0.09	3
Nos targets*	157	0.50	1.54	0.00	0.02	3
Nos tfs	34	0.43	1.23	0.16	0.12	3
Myc targets 1	207	0.33	1.29	0.10	0.09	3
Myc targets 2	703	-0.23	-1.16	0.23	0.54	3

Size, the number of genes included in the analysis; ES, the enrichment score that reflects the degree to which a gene set is overrepresented at the top or bottom of the ranked list of 19,093 genes; NES, normalized enrichment score (accounts for difference in gene-set size and can be used to compare results across gene sets; NOM *P*-val, nominal *P* value [estimates the statistical significance of the enrichment score for a single gene set; a NOM *P*-val of zero (0.0) indicates an actual *P* value of less than 1 per number-of-permutations; the number of permutation performed in our analysis was 1,000]; FDR q-val, false discovery rate q value (the estimated probability that a gene set with a given NES represents a false-positive finding; the FDR q value is adjusted for gene-set size and multiple hypotheses testing; each gene set is considered significant when the FDR is less than 25%).

*The gene set includes *ROR1*.

Table S4. Clinical pathological characteristics of patients with ovarian cancer

Sample ID	Histology type	Stage	Metastases	Prior therapy
Primary ovary				
1	Small-cell carcinoma/neuroendocrine	N/A	N/A	None
2	Clear-cell carcinoma	I	N/A	None
3	Clear-cell carcinoma	IIIC	Yes	None
4	Endometrioid carcinoma	IA	N/A	None
5	Endometrioid adenocarcinoma	I	N/A	None
6	Mixed endometrioid squamous-cell carcinoma	IIIC	Yes	None
7	Endometrioid adenocarcinoma	IIIC	Yes	None
8	Serous papillary adenocarcinoma	II	N/A	None
9	Serous papillary adenocarcinoma	IIB	N/A	None
10	Mixed Müllerian tumor/serous	IIIC	Yes	None
11	Serous papillary adenocarcinoma	IIIC	Yes	None
12	Serous papillary adenocarcinoma	IIIC	Yes	None
13	Serous papillary adenocarcinoma	IIIC	N/A	Carboplatin taxol
14	Serous papillary adenocarcinoma	IV	Yes	None
Ovary PDX				
OV1110	Carcinosarcoma, malignant mixed Müllerian tumor	N/A	N/A	None
AA1581	Serous papillary adenocarcinoma	N/A	N/A	None
AA0857	Serous papillary adenocarcinoma	N/A	N/A	Taxane/platinum

N/A, not available.